

## Article

# Microstructure and Mechanical Performance of Tin-Based Babbitt Alloy Containing Iron Oxide and Silica Nanoparticles

Mohamed Ramadan <sup>1,2,\*</sup>, Tayyab Subhani <sup>1,\*</sup>, Khalid M. Hafez <sup>2</sup>, Naglaa Fathy <sup>3</sup>, Badreddine Ayadi <sup>1,4</sup>, K. S. Abdel Halim <sup>1,2</sup>, Abdulaziz S. Alghamdi <sup>1</sup> and Khaled M. Ibrahim <sup>2</sup>

<sup>1</sup> College of Engineering, University of Ha'il, P.O. Box 2440, Hail 81481, Saudi Arabia

<sup>2</sup> Central Metallurgical Research and Development Institute (CMRDI), P.O. Box 87, Helwan 11421, Egypt

<sup>3</sup> Department of Physics, College of Science, University of Ha'il, P.O. Box 2440, Hail 81481, Saudi Arabia

<sup>4</sup> Laboratory of Applied Fluid Mechanics, Environment and Process Engineering "LR11ES57", National School of Engineers of Sfax (ENIS), University of Sfax, Route Soukra Km 3.5, Sfax 3038, Tunisia

\* Correspondence: mnrnais3@yahoo.com (M.R.); drtayyabsubhani@gmail.com (T.S.)

**Abstract:** Iron oxide and silica nanoparticles were individually incorporated in tin-based Babbitt alloy and combined to prepare a novel class of nanocomposites for bearing material applications. The route of liquid metallurgy in combination with the stirring technique was adopted to manufacture nanocomposites. Microstructural evolution and mechanical property evaluation were performed by optical and electron microscopy, EDS, hardness, compression, and wear tests. The morphology of the Cu<sub>6</sub>Sn<sub>5</sub> phase was changed from elongated to spherical in the microstructures of nanocomposites. The solitary addition of 0.5 wt% iron oxide nanoparticles improved the hardness and compressive strength but adversely affected the wear properties by increasing the weight loss and friction coefficient value. In contrast, the addition of 0.5 wt% silica nanoparticles could not significantly increase the hardness and compressive strength but it could improve the tribological properties by reducing the weight loss and friction coefficient value. Tin-based Babbitt alloy showed a compressive strength of 89.22 ± 0.50 MPa after the addition of 0.5 wt% iron oxide showing a rise of ~11%. The combined effect of the addition of both types of nanoparticles showed considerable results, i.e., a rise of ~7.9% (86.75 ± 0.68 MPa). The balanced approach of incorporating dual reinforcements of 0.25 wt% iron oxide and 0.25 wt% silica nanoparticles intermediately improved the hardness, compressive strength, and decreased weight loss.

**Keywords:** tin-based babbitt alloy; bearing material; nanocomposite; silica; iron oxide; mechanical



**Citation:** Ramadan, M.; Subhani, T.; Hafez, K.M.; Fathy, N.; Ayadi, B.; Abdel Halim, K.S.; Alghamdi, A.S.; Ibrahim, K.M. Microstructure and Mechanical Performance of Tin-Based Babbitt Alloy Containing Iron Oxide and Silica Nanoparticles. *Metals* **2023**, *13*, 324. <https://doi.org/10.3390/met13020324>

Academic Editor: Gregory Guisbiers

Received: 30 December 2022

Revised: 26 January 2023

Accepted: 31 January 2023

Published: 5 February 2023



**Copyright:** © 2023 by the authors. Licensee MDPI, Basel, Switzerland. This article is an open access article distributed under the terms and conditions of the Creative Commons Attribution (CC BY) license (<https://creativecommons.org/licenses/by/4.0/>).

## 1. Introduction

Bearings are primarily used to promote the rotating motion of counteracting parts and to control their sliding friction. The selection of bearing materials, therefore, demands careful consideration of mechanical properties such as hardness, compressive strength, tribological performance, fatigue strength, and corrosion resistance. It is well-known [1–4] that mechanical properties together with physical and functional attributes of bearing materials are significantly affected by their microstructure. Hence, a combination of structure-property assumes the prime importance in bearing materials, as is the case of all other engineering materials. Moreover, the cost of any material is the prime requisite along with a cost-effective manufacturing process. Load, shaft speed, working temperature, oil supply, and shaft hardness are the other service conditions, which should also be considered during the design and manufacturing of bearing materials [1–4].

Plain bearings are designed in internal combustion engines to convert the reciprocating motion of pistons into the rotary motion of a crankshaft. The challenge is, therefore, to produce a strong material with improved fatigue resistance. Otherwise, bearing materials may soften, de-shape, and adapt a variation in alignment [5]. Although metallic bearing materials are designed traditionally and produced through conventional traditional

manufacturing techniques, the dream for high quality, high reliability, and long service life-bearing materials has not yet been achieved. Moreover, other factors including load, lubrication, temperature, arrangement, mounting, noise, and environmental condition are should be carefully examined to meet the desired criteria. Typically, journal and thrust bearings are fabricated by bonding two dissimilar materials named bimetallic materials. The quality of bearings and their performance are governed by the material design of the working layer as well as fabrication techniques [6–10].

Generally, bearing materials are classified into three main groups: (a) white metals (tin-based and lead-based alloys, Babbitt), (b) copper-tin-lead alloys, and (c) aluminum-tin-lead alloys. For low-speed diesel engines, white metal (Babbitt) has promising properties such as superior antifriction property, emergency running capabilities, and conformability as compared to other bearing materials. Tin-based alloy is a low melting point alloy with a multiphase microstructure containing a soft matrix with uniform distribution of hard precipitates. Moreover, embeddability and seizure resistance in tin-based bearing alloys is achieved through the soft matrix while high hardness, strength, and the supporting role in working load is achieved by hard precipitates [11–14].

Although Cu-alloys, Sn-based alloys, and Al-alloys have been extensively investigated for bearing applications, most of the previous studies have focused on improving wear resistance by elemental additions, micro/nanoparticle incorporation including carbon nanotubes, and modification in manufacturing processes [15–19]. A few studies [16,17] were also devoted to optimizing and understanding the wear mechanism of bearing materials with metal and ceramic nanoparticle reinforcements for heavy duty and high-performance applications. Although tin-based Babbitt alloys are called super materials for sliding bearing applications, especially for journal and thrust bearings, their carrying load capacity is low (~5.5–10.5 MPa) compared with other commercially available bearing materials like bronzes and aluminum alloys [20,21]. Tin-based Babbitt alloys are soft materials with a relatively low hardness of ~24.2 BHN; despite this fact, tin-based Babbitt alloys are commonly used as bearing materials in journal and thrust bearing applications, especially for the components of steam turbines, engines, and compressors. Sb and Cu are added in varying quantities to develop the desired microstructure for required properties. These materials have high wear and corrosion resistance, good run-in properties, and good behavior in the absence of sufficient lubrication. Moreover, common production techniques are employed for depositing the tin-based Babbitt alloys onto a supporting bearing shell like centrifugal casting, gravity static casting, arc spraying, and TIG welding [7,9,22–24].

Tin-based bearing alloy microstructure consists of a soft solid solution matrix and two hard intermetallic phases, i.e., SbSn and Cu<sub>6</sub>Sn<sub>5</sub>. The Sn–Sb–Cu alloy is widely used for sliding bearings operating in wet oily conditions. The microstructures of Sn-based bearing alloys vary according to the loading fraction of Sb and Cu in Sn [25]. To improve tin-based bearing alloy structures and their bonding with supporting external shells, different technologies are in vogue like casting, welding, cladding, and thermal spraying [26–28]. For all previous processing techniques, macro/microstructure, porosity, hardness, wear behavior, and bonding strength between tin-based bearing alloys and external shell together with the appearance of segregations are characterized. Other research directions focus on the improvement of bearing materials by powder metallurgy and stir casting techniques involving MgO reinforcement [29–31]. Al<sub>2</sub>O<sub>3</sub> particles coated with Y<sub>2</sub>O<sub>3</sub> and ferrochromium slag were also added in aluminum using the squeeze casting method for the improvement of mechanical properties and wear resistance [29–31]. Both fatigue strength and wear resistance of tin-based bearing materials were significantly increased by the size morphology of the CuSn ( $\eta$ ) and SnSb ( $\beta$ ) hard phases in the soft matrix.

For its availability, high heat stability, low cost, as well as excellent electrical and magnetic properties, iron oxide is widely used in industry for its potential applications in a variety of fields. Iron oxide nanoparticle is a promising additive to enhance the properties of the free solder alloys' reinforcement phase [32,33]. A previous study [34] reported that the addition of Fe<sub>2</sub>O<sub>3</sub> nanoparticles significantly improves the wettability of free lead Sn

solder alloys and inhibits the growth and formation of interfacial IMCs. Silica nanoparticles have many biological and industrial applications for its excellent biocompatibility, thermal stability, low toxicity, and large-scale synthetic availability [35,36]. The performance of semiconductors, coatings, and metal matrix composites are significantly improved with the addition of SiO<sub>2</sub> nanoparticles. Silica nanoparticles are potential reinforcement particles that enhance the creep resistance and mechanical properties of free lead soldering alloys [37,38].

Although tin-based bearing alloys have been widely used in bearing components for automotive, steam turbines, compressors, and shipbuilding industries due to their better friction properties, corrosion resistance, and high thermal conductivity [39,40], still, the improvement in properties is urgently required to increase loading capacity and compression strength for heavy duty and high-performance bearing applications.

Nanoparticle reinforcement enhances mechanical properties, especially the wear and corrosion resistance of the matrix materials in tin-based Babbitt alloys. These materials possess an excellent strength-to-weight ratio and are currently replacing conventional alloys and traditional metal matrix composites in many new and existing designs. At the same time, the addition of hard nano-ceramic reinforcements like SiC and Al<sub>2</sub>O<sub>3</sub> may harm and scratch the smooth surface of the metallic shaft supported by tin-based Babbitt alloy bearings [15,16]. Therefore, this project is designed to develop and adopt a strategy of novel incorporation of nanoparticles with moderate hardness and strength for heavy duty and high carrying load capacity applications. Iron oxide and silica nanoparticles were added individually and in combination to explore their solitary and hybrid effects on the microstructural and mechanical properties of tin-based Babbitt alloys for targeted applications of bearing materials without damaging the counter metallic shafts.

## 2. Materials and Methods

In the present investigation, four sets of specimens were prepared. The first set was comprised of reference specimens without the addition of any nano-reinforcements. The second set was comprised of nanocomposite specimens containing 0.5 wt% silica nanoparticles while the third set consisted of nanocomposite specimens containing 0.5 wt% iron oxide nanoparticles. The fourth set contained hybrid nano-reinforcement specimens containing binary nano-reinforcements of silica and iron oxide nanoparticles at the loading of 0.25 wt% each, thus making it equal to the total loading of 0.5 wt%.

Silica nanoparticles of spherical morphology and average particle size of ~20 nm and iron oxide nanoparticles of spherical morphology and average particle size of ~95 nm were used as nano-reinforcement, as synthesized and procured from Centre of Nanomaterials (Beni-Suef University, Beni Suef 62521, Egypt). Figure 1 shows the SEM images of iron oxide and silica nanoparticles. Second grade tin-based Babbitt alloy was used as the matrix material to prepare nanocomposites, as procured from Rotometals, San Leandro, CA, USA.

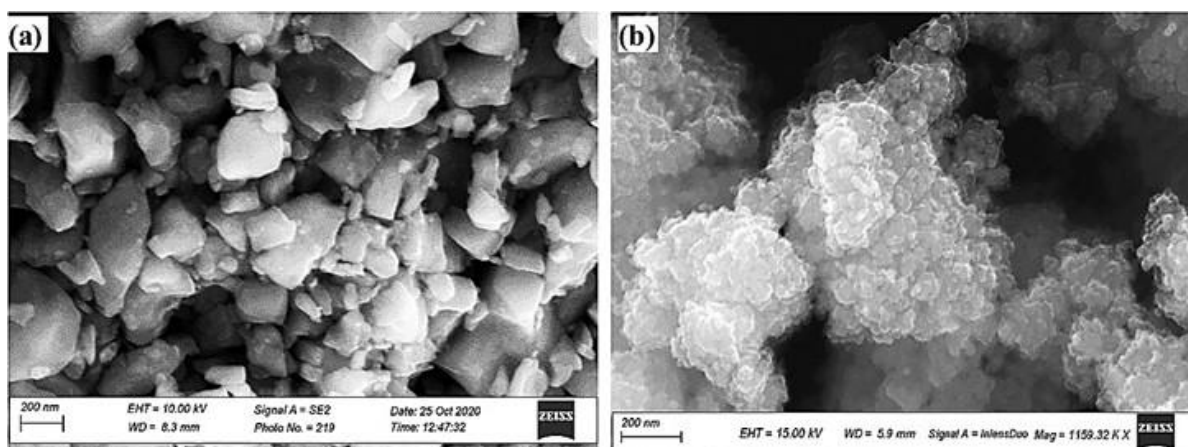
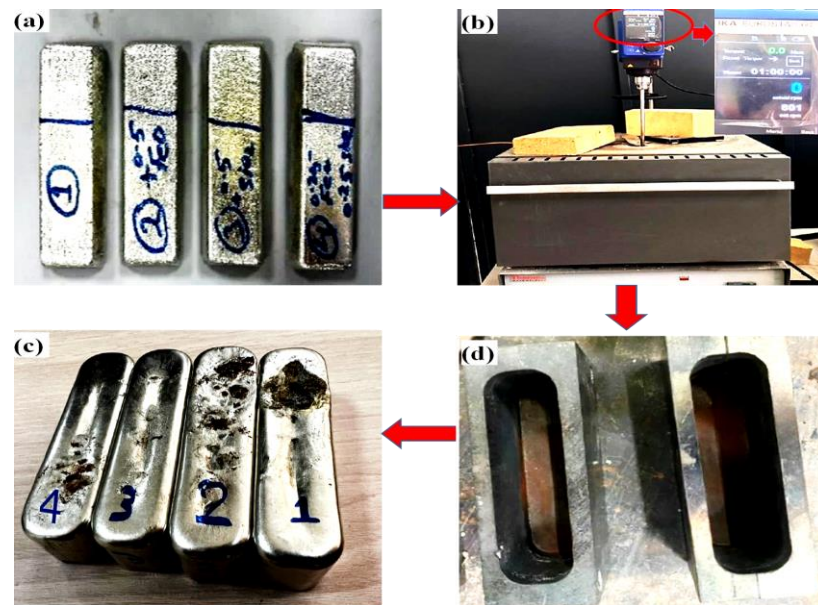


Figure 1. SEM photographs of (a) Fe<sub>2</sub>O<sub>3</sub> and (b) SiO<sub>2</sub> nanoparticles.

To prepare nanocomposites, a charge of 500 g was prepared containing 99.5 wt% tin-based Babbitt alloy and 0.5 wt% silica nanoparticles in a graphite crucible in an electrical muffle furnace attached with a stirring mechanism comprising a two-blade impeller. The furnace was heated to a temperature of 400 °C with a heating rate of 10 °C/min. As the melting point of tin-based Babbitt alloy was 375 °C, the maximum heating temperature of the charge was kept at 400 °C thus providing a superheat of 25 °C. The tin-based Babbitt alloy was first loaded into the crucible and after heating it to 400 °C, the silica nanoparticles wrapped in aluminum foil were immersed into molten charge for their convenient incorporation and heated at 400 °C for 20 min. During the holding time, the stirring operation was continuously performed after the addition of nanoparticles. The stirring was performed at a speed of 800 rpm. During the heating cycle, argon gas was flowing in the furnace to avoid unnecessary oxidation of the charge. After heating, holding, and stirring the charge to the desired parameters, the molten charge was poured on a pre-heated metallic mold at 175 °C. Figure 2 shows the received tin-based Babbitt bars, muffle furnace with mechanical stirrer, metallic mold, and fabricated nanocomposites specimens for pre-paring nanocomposites Babbitt. The same process was repeated for the other three sets of specimens. For a reliable comparison, the reference specimens without nano-reinforcements were passed through the same operation of heating, holding, and stirring. The dimensions of the cast specimens were length 90 mm, width 28 mm, and height 25 mm.



**Figure 2.** As received tin-based Babbitt bars (a), muffle furnace with mechanical stirrer (b), metallic mold (d), and fabricated nanocomposites specimens (c) for preparing nanocomposites Babbitt.

Optical and scanning electron microscopy (SEM) was performed to observe the microstructures of specimens under an optical microscope (Image Analyzer Software, Olympus GX51, Tokyo, Japan version) and a scanning electron microscope (FEI Quanta 250 SEM, Eindhoven, The Netherlands). Optical micrographs were captured at two different magnifications: 200 $\times$  and 500 $\times$ . SEM images were acquired in the secondary electron imaging mode at an accelerating voltage of 10 and 20 kV. The chemical compositions of the tin-based Babbitt alloy were performed using an energy-dispersive X-ray spectroscopy (EDAX-AMETEK, Mahwah, NJ, USA).

Metallographic preparations were performed on specimens prior to observation under microscopes, which involved cutting, grinding, polishing, and etching the specimens. The specimens were ground with SiC emery papers of grit size 320, 600, 800, 1200, 1500, which was followed by polishing the specimens using alumina powder of size 1.0  $\mu\text{m}$ . After the

polishing process, the etching of the specimens was performed with nital (2% HNO<sub>3</sub> and ethyl alcohol) with an immersion time of about 30 s.

A microhardness tester (VLS 3853, Shimadzu, Japan) was used to perform hardness tests using a load of 200 g for the dwell time of 5 s; at least, five values at different locations were taken from each specimen to obtain average value. For compression testing, a universal testing machine (Instron 5969, Instron with a maximum load of 50 KN, Norwood, MA, USA), was employed at a strain rate of 1 mm/min. At least five tests of each specimen were performed while the size of the specimens was diameter 12.5 mm and height 25 mm (L/D = 2) (ASTM E9, Compression Testing of Metallic Materials at Room Temperature). Tribological testing was performed on a T-01M pin-on-disk tribotester under dry friction conditions. The specimens served as the pin while the counterbody acted as the rotating disk. The rotational speed of the disk was 149 rpm while the sliding velocity and distance were 0.25 m/s and 150 m, respectively. The applied pressure was 1 MPa with the test duration of 10 min at room temperature of 25 °C. The specimen pins and rotating disks were ultrasonically cleaned with acetone and dried in hot air to obtain clean surfaces before the tribological experiments. The friction coefficient values were automatically recorded under steady state sliding conditions. The profiles of the worn specimen surfaces were measured on a surface profiler and the wear volume was automatically calculated by the machine. The wear rates were calculated using the wear volume and sliding distance. At least three specimens were tested under identical conditions to acquire average values. Technical drawings of the specimen pin and the rotating disk are given in Figure 3.

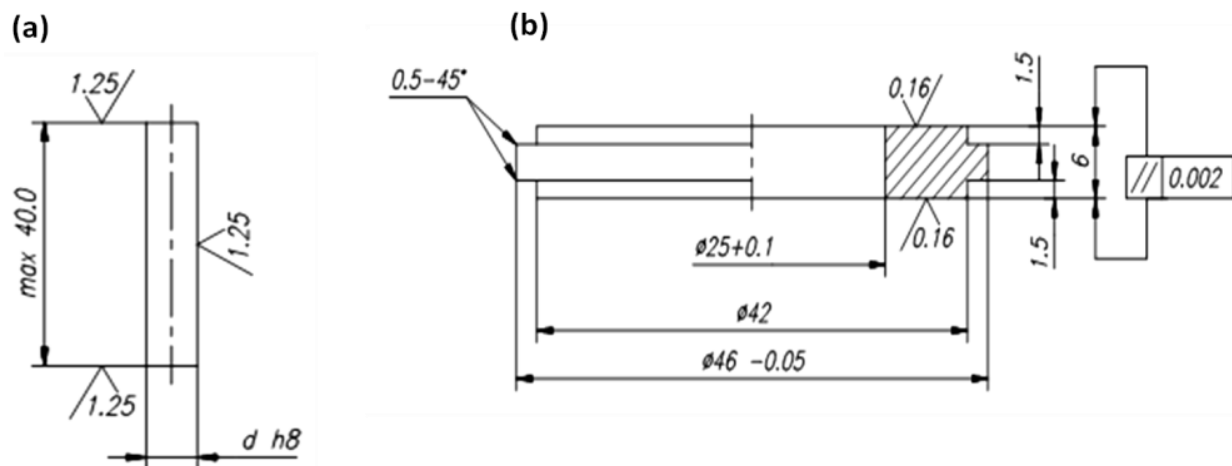


**Figure 3.** Technical drawings of (a) specimen and (b) rotating disk used in tribological test.

### 3. Results and Discussion

#### 3.1. Microstructural Evolution

The SEM of the Sn-Based Babbitt microstructure used as the matrix in the present study is shown in Figure 4. The image clearly reveals the presence of Cu<sub>6</sub>Sn<sub>5</sub> and SbSn phases in the matrix of the SnSbCu solid solution. The size of the Cu<sub>6</sub>Sn<sub>5</sub> phase is comparatively larger than the SbSn phase and corresponds to the shape of needles and asterisks. Such a microstructure comprising a solid solution matrix with hard binary phases makes a hybrid metal matrix composite with good fatigue properties [17–19]. Literature shows that the variation in the chemical composition of tin-based Babbitt alloy changes the microstructure: less than 8 wt% Sb distributes Cu<sub>6</sub>Sn<sub>5</sub> and SbSn phases more uniformly while the presence of Sb greater than 8 wt% shows primary cuboid SbSn phase [20–22]. Figure 5 shows the SEM and EDS elemental mapping of tin-Based Babbitt alloy: a fair distribution of Sb, Sn, and Cu can be witnessed in different phases of the Babbitt alloy in the EDS analysis.

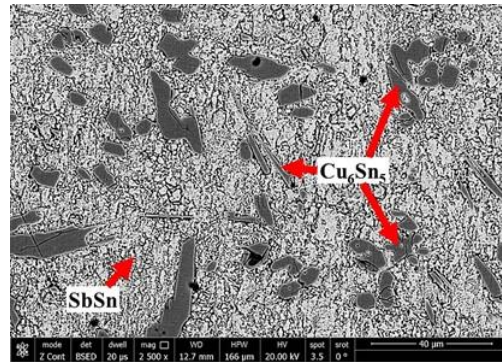


Figure 4. SEM of Sn-Based Babbitt alloy microstructure used as the matrix.

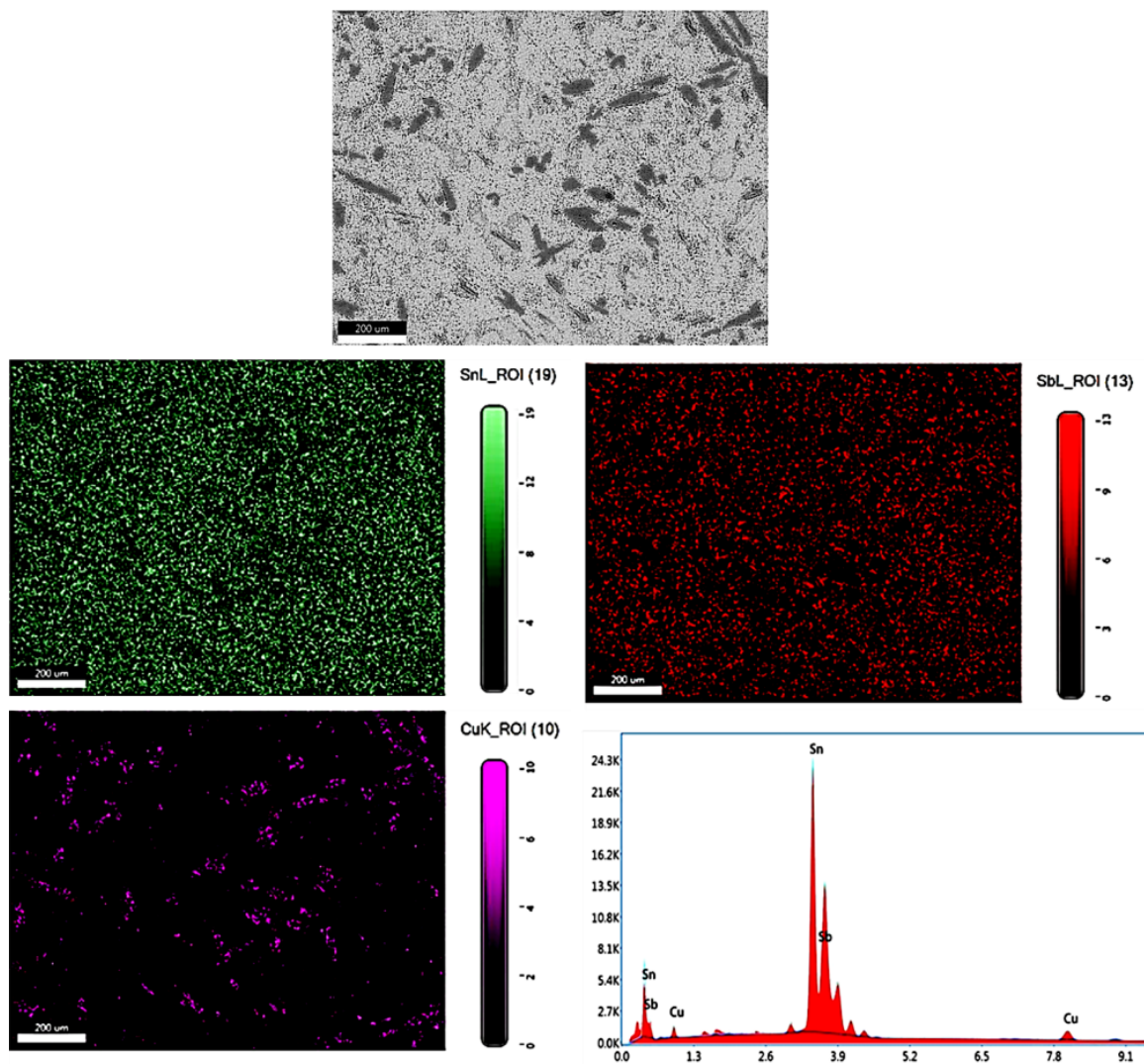
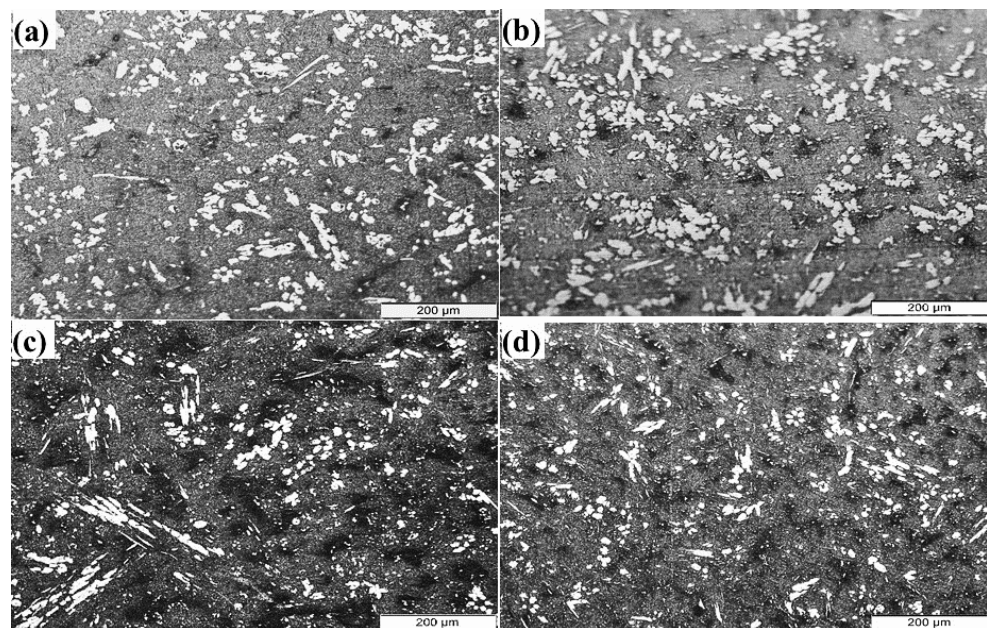


Figure 5. SEM and EDS element mapping analysis of Sn-Based Babbitt alloy.

Figure 6 show the optical micrographs of tin-based Babbitt alloy with and without the addition of nanoparticles. The features of the optical micrograph of reference tin-based Babbitt alloy in Figure 6a are the same as shown in Figures 4 and 5. The presence of the  $\text{Cu}_6\text{Sn}_5$  and  $\text{SbSn}$  phases is visible in the matrix of the  $\text{SnSbCu}$  solid solution and the needle-like and asterisk-like shape of the  $\text{Cu}_6\text{Sn}_5$  phase can be clearly seen, which also confirms the presence of less than 8 wt% Sb in the alloy, as discussed earlier. The addition

of 0.5 wt% iron oxide has a minor effect on the modification in microstructure or change in the shape and morphology of phases (Figure 6b) while the incorporation of 0.5 wt% silica nanoparticles has changed the morphology of the  $\text{Cu}_6\text{Sn}_5$  phase from needle-like to fine globular structure (Figure 6c). It can be inferred that under the same loading fraction of two types of nanoparticles, the quantity of nanoparticles of silica is greater due to their smaller size, i.e., 20 nm in comparison to the iron oxide nanoparticle size of 95 nm. The presence of the smaller size of nanoparticles of silica may have restricted the growth of the  $\text{Cu}_6\text{Sn}_5$  phase and also modified its shape. This is the reason why, in hybrid composite, the morphology change of  $\text{Cu}_6\text{Sn}_5$  phase was also observed (Figure 6d) although the needle-like structure is simultaneously present with fine globular structure due to reduced quality of silica nanoparticles, i.e., 0.25 wt% in combination with equal loading fraction of iron oxide nanoparticles.



**Figure 6.** Optical micrographs of tin-based Babbitt alloy: (a) without nanoparticle addition, (b) 0.5 wt% iron oxide nanoparticles, (c) 0.5 wt% silica nanoparticles, and (d) 0.25 wt% iron oxide and 0.25 wt% silica nanoparticles.

A uniform distribution and refining of the main  $\text{Cu}_6\text{Sn}_5$  phase in the Sn matrix (see Figure 6d) that is associated with a uniform dispersion of nanoparticles is essential for improved mechanical performance of nanocomposites. A homogenous presence of matrix precipitates was noted in nanocomposites containing 0.5 wt% silica nanoparticles and dual incorporation of iron oxide and silica nanoparticles at equal incorporation of 0.25% each (Figure 6d).

SEM images of tin-based Babbitt alloy with and without the addition of nanoparticles are shown in Figure 6. A significant change in the morphology of the  $\text{Cu}_6\text{Sn}_5$  phase was observed, which changed from elongated in reference specimen to spherical in nanocomposite specimens. An interesting feature is the presence of cracks in the elongated  $\text{Cu}_6\text{Sn}_5$  phase in reference specimen (Figure 7a), which is absent in nanocomposite specimens (Figure 7b–d). It is still not clear whether these cracks were produced during the solidification of reference material or were developed during the polishing process of the specimen. Nevertheless, these cracks are absent in nanocomposite specimens, which is a promising effect of the incorporation of nanoparticles. The change in the morphology of the  $\text{Cu}_6\text{Sn}_5$  phase from large elongated size to small spherical shape should influence the mechanical properties, as discussed further below.

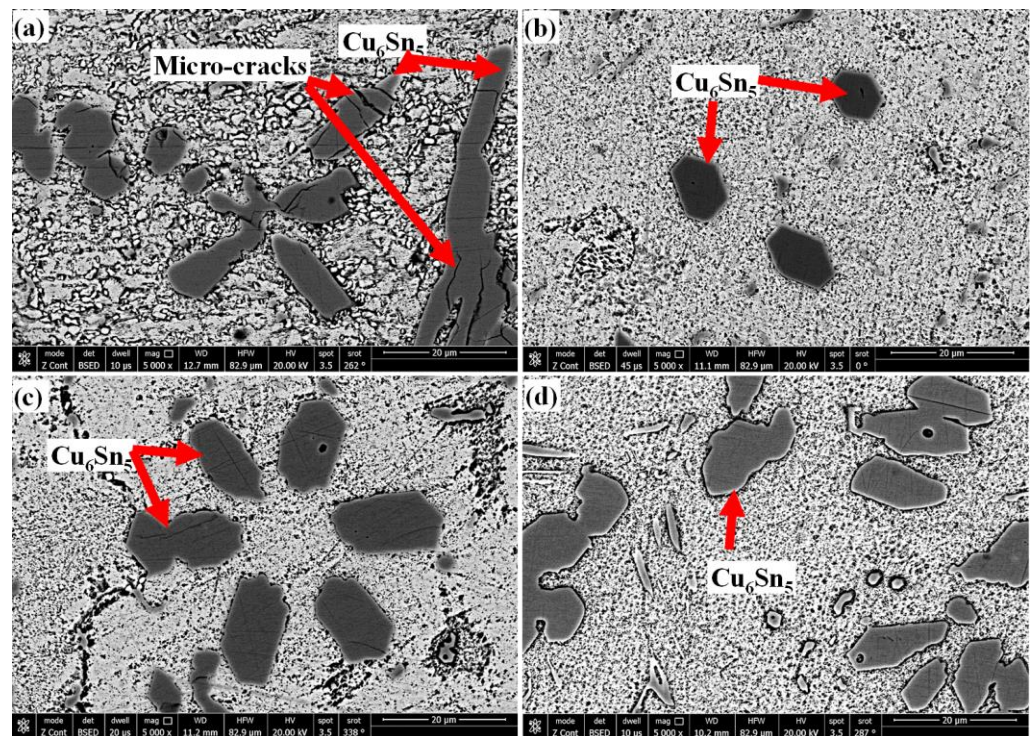


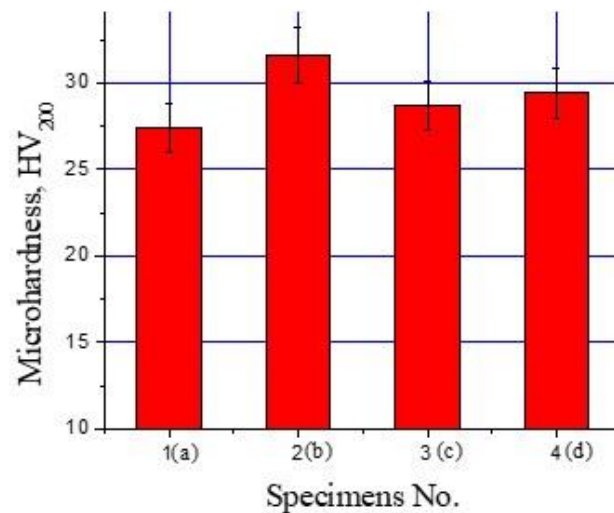
**Figure 7.** SEM images showing the morphology of  $\text{Cu}_6\text{Sn}_5$  phase in tin-based Babbitt alloy (a) without nanoparticle addition, (b) 0.5 wt% iron oxide nanoparticles, (c) 0.5 wt% silica nanoparticles, and (d) 0.25 wt% iron oxide and 0.25 wt% silica nanoparticles.

At the given magnification of these SEM images, it is difficult to identify the nanoparticles. Nevertheless, it can be expected that the incorporation of nanoparticles at second phase may decrease the grain size of the matrix material and thus increase the hardness, as discussed below. The nanoparticles are expected to gather at the grain boundaries thus providing a pinning effect and restriction of grain growth. The effect of decreased grain size is expected to emerge both in hardness and in compressive properties.

### 3.2. Mechanical Properties

The hardness values of the reference tin-based Babbitt alloy and its nanocomposites are plotted in Figure 8. It is evident from the figure that the incorporation of nanoparticles, both individually and combined, increased the hardness of Babbitt alloy; however, the effect of their addition was different in three nanocomposite specimens. Reference specimen of tin-based Babbitt alloy showed a value of  $27.4 \pm 1.37$  HV, which increased to  $31.6 \pm 1.58$  HV after the addition of 0.5 wt% iron oxide showing a rise of  $\sim 15\%$ . In comparison, the effect of the incorporation of silica on tin-based Babbitt alloy was less, i.e.,  $28.7 \pm 1.44$  HV, thus revealing an increase of only  $\sim 4.7\%$ . As expected, the combined effect of the addition of both types of nanoparticles showed intermediate results, i.e., a rise of  $\sim 7.3\%$  ( $29.4 \pm 1.47$  HV).

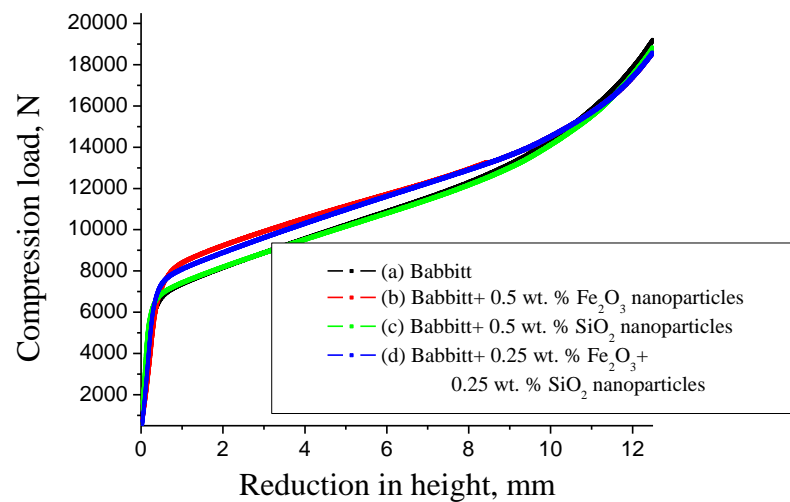
The modification in the morphology of the hard  $\text{Cu}_6\text{Sn}_5$  phase and its uniform distribution is the primary reason for high hardness. A secondary effect may be due to the change in the morphology of the hard  $\text{Cu}_6\text{Sn}_5$  phase along with the absence of  $\text{Cu}_6\text{Sn}_5$  phase agglomerates, as discussed elsewhere [16]. In our previous study [16], an increased hardness ( $\sim 20\%$ ) was noticed after the addition of the same loading fraction of nanoparticles of alumina, i.e., 0.5 wt%. This comparative rise in the hardness values of nanocomposites containing alumina nanoparticles may be attributed to the high hardness value of alumina. Nevertheless, considering the rule of mixtures, the hardness of the nanocomposites in the present study was up to expectations.



**Figure 8.** Hardness of tin-based Babbitt alloy and nanocomposites: (a) Babbitt alloy and nanocomposites containing (b) 0.5 wt% iron oxide nanoparticles, (c) 0.5 wt% silica nanoparticles, and (d) 0.25 wt% iron oxide and 0.25 wt% silica nanoparticles.

Another reason for the increase in hardness in nanocomposites may be the grain size reduction after adding nanoparticles. The size of silica nanoparticles is smaller than iron oxide nanoparticles in the present study and the effect of smaller size nanoparticles should have been significant in comparison to larger size nanoparticles, as observed elsewhere [41]. However, in the current investigation, the composition, morphology, and shape of the two nanoparticles are different, along with the difference in their nanometer size. The dissimilarity in composition and morphology of the two types of nanoparticles dominated the size effect, which was also observed in a separate study [42] where the same nanoparticle material was used with a change in nanoparticle size. It can also be hypothesized that the grains encapsulated the small size (20 nm) silica particles during their development and growth, and thus, a significant effect of grain size reduction may not emerge. In contrast, large size (~95 nm) of iron oxide together with their irregular shape may have truly influenced the grain refinement. This effect, along with the direct effect of the incorporation of iron oxide nanoparticles, actually increased the hardness of nanocomposites containing iron oxide nanoparticles.

Figure 9 displays the compressive test results of tin-based Babbitt alloy nanocomposites with and without nanoparticles; the figure typically shows the compression load as a function of reduction in specimen height. It can be seen that the addition of 0.5 wt% iron oxide nanoparticles showed a greater effect in increasing the compression load than silica nanoparticles. The solitary incorporation of 0.5 wt% iron oxide nanoparticles revealed the maximum value in nanocomposites while their half quantity, i.e., 0.25 wt%, in hybrid nanocomposites together with 0.25 wt% silica nanoparticles still had a greater effect than the individual addition of silica nanoparticles at the loading fraction of 0.5 wt%. Although the nanocomposite containing 0.5 wt% silica nanoparticles showed a comparative rise in compression load, it is not significantly high enough to justify the addition of nanoparticles. Nevertheless, it can be expected that the reinforcement of increased quantities of silica nanoparticles may offer substantial improvement. Similarly, further rise in compression strength can be achieved after the addition of iron oxide nanoparticles in quantities greater than 0.5 wt%.



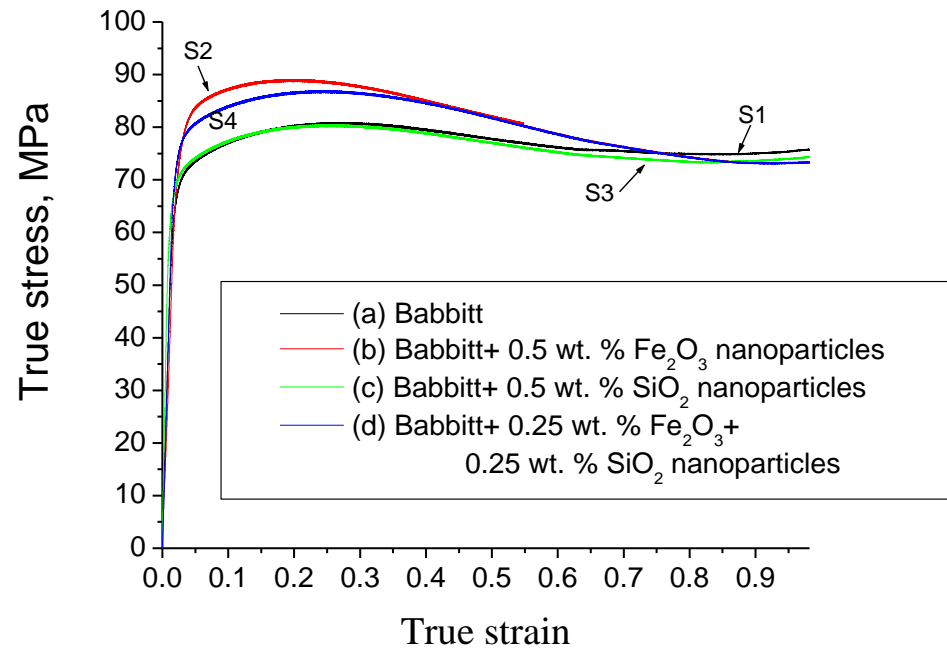
**Figure 9.** Compression load as a function of reduction in specimen height in tin-based Babbitt alloy (a) without nanoparticle addition, with (b) 0.5 wt% iron oxide nanoparticles, (c) 0.5 wt% silica nanoparticles, and (d) 0.25 wt% iron oxide and 0.25 wt% silica nanoparticles.

Figure 10 shows the true stress-strain diagram of tin-based Babbitt alloy nanocomposites with and without nanoparticles; indeed, the nanocomposite containing 0.5 wt% iron oxide nanoparticles showed the maximum compressive strength followed by the hybrid nanocomposite containing both 0.25 wt% iron oxide and 0.25 wt% silica particles. The compressive strength of nanocomposite containing 0.5 wt% silica nanoparticles is still higher than the reference tin-based Babbitt alloy specimen. Reference specimen of the tin-based Babbitt alloy showed a compressive strength value of  $80.38 \pm 0.58$  MPa, which increased to  $89.22 \pm 0.50$  MPa after the addition of 0.5 wt% iron oxide showing a rise of  $\sim 11\%$ . In comparison, there is no significant effect of the incorporation of silica nanoparticles on tin-based Babbitt alloy. The combined effect of the addition of both types of nanoparticles showed considerable results, i.e., a rise of  $\sim 7.9\%$  ( $86.75 \pm 0.68$  MPa). The mechanical property results obtained in both hardness and compression tests complement each other, i.e., the effect of iron oxide nanoparticles on the mechanical performance of nanocomposites is higher than silica nanoparticles while the hybrid nanocomposites provide an intermediate rise in mechanical properties.

In a different study, the increase in tensile strength was noticed after adding nanoparticles of ilmenite ( $\text{FeTiO}_3$ ) [42]. Similarly, in the present study, an increase in tensile strength is expected although the characterization was performed only for compression tests. In a separate study [43], nickel-coated graphite particles were incorporated in the Babbitt alloy up to 10 wt%: a continuous increase in hardness was observed until the loading of 8 wt%, after which a downward trend was observed owing to the agglomeration of particles. The formation of cracks at the nickel-coated graphite-concentrated boundaries was found to be the possible reason for the decline in hardness values. No such effect was observed in the present study due to the absence of nickel, which developed the  $\text{Ni}_3\text{Sn}_4$  phase in the other investigation.

The friction coefficients of tin-based Babbitt alloy nanocomposites with and without the addition of nanoparticles for a duration of 10 min (600 s) are shown in Figure 11 and friction coefficient values are given in Table 1. It can be seen that the friction coefficient values ranged between 0.35 and 0.40, which matches the literature [24]. Moreover, the values increased with the addition of nanoparticles, wherein a significant rise was noticed after the incorporation of iron oxide nanoparticles. The reference specimen of pure tin-based Babbitt alloy showed a value of 0.352, which significantly increased to 0.396 after the addition of 0.5 wt% iron oxide particles. However, the effect of the incorporation of 0.5 wt% silica nanoparticles was not considerable, i.e., 0.354. The hybrid nanocomposite specimen showed a value close to that containing iron oxide nanoparticle, i.e., 0.399. In

contrast, in another study, the friction coefficient was found to unceasingly decrease after the continuous rise of the soft material as reinforcement, i.e., nickel-coated graphite, which acted as the solid lubricant [43].



**Figure 10.** Compression stress-strain diagram of tin-based Babbitt alloy (a) without nanoparticle addition, with (b) 0.5 wt% iron oxide nanoparticles, (c) 0.5 wt% silica nanoparticles, and (d) 0.25 wt% iron oxide and 0.25 wt% silica nanoparticles.

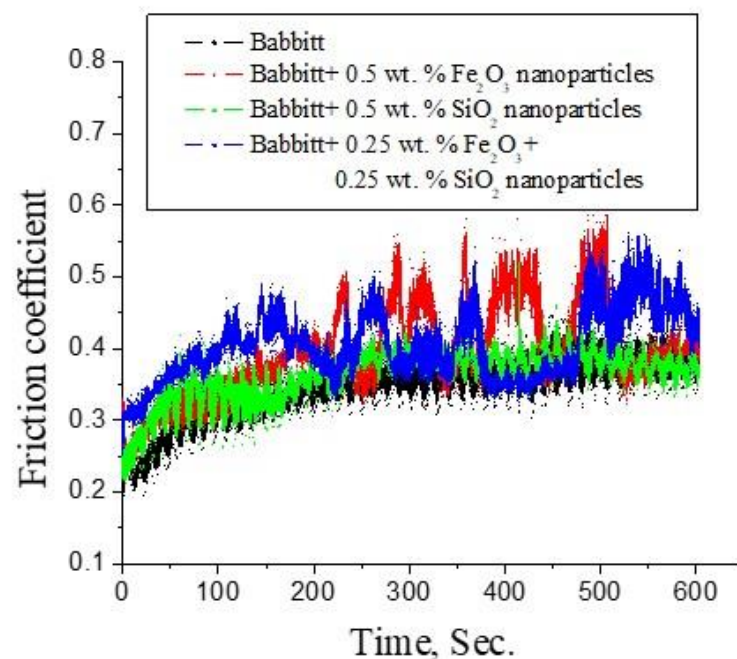


**Figure 11.** The friction coefficients of tin-based Babbitt alloy nanocomposites with and without the addition of nanoparticles.

**Table 1.** Weight loss and friction coefficient values of tin-based Babbitt alloy nanocomposites with and without nanoparticles.

No.	Additions	Weight Loss (g)	Friction Coefficient
S1	Babbitt alloy	0.00819 ± 000024	0.352
S2	Babbitt + 0.50% Fe <sub>2</sub> O <sub>3</sub> nanoparticles	0.00830 ± 000015	0.396
S3	Babbitt + 0.50% SiO <sub>2</sub> nanoparticles	0.00810 ± 000005	0.364
S4	Babbitt + 0.25% Fe <sub>2</sub> O <sub>3</sub> + 0.25% SiO <sub>2</sub> nanoparticles	0.00800 ± 000008	0.399

After the wear test, the weight loss values were measured, which are presented in Table 1. The reference specimen of pure tin-based Babbitt alloy showed a value of 0.00819 g, which increased to 0.00830 g after reinforcing 0.5 wt% iron oxide nanoparticles. However, the addition of 0.5 wt% silica nanoparticles reduced the value to 0.00810, which is also lower than that of the reference specimen. Surprisingly, the dual reinforcement of iron oxide and silica nanoparticles further decreased the value to 0.00800. It can be hypothesized that during the sliding process, the silica nanoparticles were compressed and further embedded in the matrix material, and thus, decreased wear loss. In contrast, due to the large size of iron oxide nanoparticles, these were pulled-out of the specimen surface thus further increasing the weight loss owing the presence of cavities. Furthermore, the loading fraction of 0.5 wt% iron oxide nanoparticles could have promoted the agglomeration in the nanocomposites, which acted as defects in the material. At a low loading of 0.25 wt% iron oxide paired with 0.25 wt% silica nanoparticles, this effect of iron oxide nanoparticle agglomeration was subdued, thereby reducing the wear loss. One may argue upon the significant rise in hardness and compressive strength of nanocomposites containing iron oxide nanoparticles in the presence of nanoparticle agglomeration. A possible explanation is that the compressive load is applied during both the hardness and compression tests, which generally closes the defects and the decrease in strength is truly revealed in tensile testing. Nevertheless, to verify this issue, tensile testing of the nanocomposites prepared in the present study is required.

A high sliding velocity of 0.25 m/s was used in the present study, which generates frictional heat at the contact surface. It has been claimed in a previous study [43] that the generation of high frictional heat at a sliding speed of 0.2 m/s promotes a lubricating effect between the specimen and the counterbody and avoids the worn surface from further wear. However, a further rise in speed excessively softens the material surface and promotes severe wear. It can be expected that the addition of silica nanoparticles restricted the rise in excessive temperature, and thus, controlled the wear loss. However, the pull-out effect of iron oxide due to their large size dominated during sliding without controlling the weight loss.

At the sliding speed chosen in the current wear tests (0.25 m/s), the worn surfaces are characterized by microgrooves and fatigue wear, as also observed elsewhere [43,44]. However, at higher sliding velocities, severe plastic deformation and delamination are expected, which were absent in the specimens. Moreover, excessive material removal and cracks are also found perpendicular to the sliding motion, which were also missing in the specimens, except in nanocomposite specimens containing solitary iron oxide nanoparticles, wherein material removal in the form of nanoparticle pull-out might be possible.

Previous studies [16,43] on Babbitt material with sufficient strength and a lower friction coefficient can be obtained through the addition of both nickel-coated graphite particles and alumina nanoparticle. The tensile strength and interfacial bonding were improved for Babbitt by reinforcement by 0.25 wt% and 0.50 wt% nanoparticles. Other attempts [24,44,45] focused on processes' parameters and testing conditions optimization for improving the wear properties of Babbitt alloys. Babbitt alloy (B88) rubbing with a both steel ball and a Si<sub>3</sub>N<sub>4</sub> ball show a low wear resistance at dry friction conditions [24]. By increasing the pressure load from 40 to 50 N, the count of a zone emergent from the

Babbitt/aluminum–Al<sub>2</sub>O<sub>3</sub> skeleton resulted in an increase of the COF by 128.7% [44]. For a friction stirred surface modified Babbitt (B89), there was an increase in tool rotation speed from 280 to 560 RPM, and the friction coefficient and the weight loss decreased by about 30%. Otherwise, flexural strength was increased from 123 to 307 MPa [45].

Nanoparticles and dendritic growth interaction during solidification is more effective of a tool to explain the strengthening mechanism. The fine second phase particles are used as the heterogeneous nucleation sites for the crystalline primary phase resulting in increasing the nucleation process. Otherwise, the other nanoparticles that are not shared in nucleation will be restricted in the dendrites and absorbed at the front of the liquid–solid interface, which hinders the dendrites' growth and realizes the solidification microstructure refinement [46,47].

#### 4. Conclusions

Novel nanocomposites of a bearing material, i.e., tin-based Babbitt alloy, were prepared by reinforcing iron oxide and silica nanoparticles, both individually and in combination. A cost-effective course of liquid metallurgy together with stirring technique was chosen to manufacture nanocomposites. The individually reinforced nanocomposite had a loading fraction of 0.5 wt% while the hybrid nanocomposite had a singular incorporation of the two nanoparticles at the loading fraction of 0.25 wt% each, thus matching the reinforcement fraction to that of individually incorporated nanocomposites. The microstructural modification was assessed by both optical and electron microscopy along with EDS while mechanical performance was evaluated by hardness, compression, and wear tests. The morphology of Cu<sub>6</sub>Sn<sub>5</sub> precipitates changed from elongated to spherical shape in the microstructures after the addition of nanoparticles. The hardness and compressive strength increased after the individual incorporation of 0.5 wt% iron oxide nanoparticles while wear properties decreased by increasing the weight loss and friction coefficient value. The hardness of the Babbitt matrix composite shows a maximum value of  $31.6 \pm 1.58$  HV by the addition of 0.5 wt% iron oxide to Babbitt alloy. The combined effect of the addition of both types of nanoparticles showed intermediate results, i.e., a rise of ~7.3% ( $29.4 \pm 1.47$  HV). Babbitt alloy showed a compressive strength of  $89.22 \pm 0.50$  MPa after the addition of 0.5 wt% iron oxide showing a rise of ~11%. The combined effect of the addition of both types of nanoparticles showed considerable results, i.e., a rise of ~7.9% ( $86.75 \pm 0.68$  MPa). The binary addition of the nanoparticles of 0.25 wt% iron oxide and 0.25 wt% silica adequately improved the hardness, compressive strength, and wear properties.

**Author Contributions:** Conceptualization, M.R., N.F., and T.S.; methodology, M.R. and T.S.; formal analysis, K.M.H.; investigation, N.F., K.M.H., B.A., and A.S.A.; resources, A.S.A. and K.M.I.; data curation, B.A. and K.S.A.H.; writing—original draft preparation, T.S.; writing—review and editing, M.R., N.F., and K.S.A.H. All authors have read and agreed to the published version of the manuscript.

**Funding:** This research has been funded by Scientific Research Deanship at University of Ha'il—Saudi Arabia through project number RG-21097.

**Data Availability Statement:** Data is contained within the article.

**Conflicts of Interest:** The authors declare no conflict of interest.

#### References

1. Kamal, M.; Mazen, S.; El-Bediwi, A.B.; El-Naggar, M. Structure, mechanical and electrical transport properties of low-melting half bearing metal alloys rapidly solidified from melt. *Radiat. Eff. Defects Solids* **2002**, *157*, 467–474. [[CrossRef](#)]
2. Tasgin, Y. The Effects of Boron Minerals on the Microstructure and Abrasion Resistance of Babbitt Metal (Sn–Sb–Cu) Used as Coating Materials in Hydroelectric Power Plants. *Int. Metalcast.* **2022**, *14*, 257–265. [[CrossRef](#)]
3. Kamal, M.; Bakr El-Bediwi, A.; El-Shobaki, M.R. Influence of alloying elements on structure and some physical properties of quenched Sn–Sb alloy. *Radiat. Eff. Defects Solids* **2006**, *161*, 549–557. [[CrossRef](#)]
4. Thomson, J.; Zavadil, R.; Sahoo, M.; Dadouche, A.; Dmochowski, W.; Conlon, M. Development of a Lead-Free Bearing Material for Aerospace Applications. *Int. Metalcast.* **2010**, *4*, 19–30. [[CrossRef](#)]

5. Zhang, Y.; Tudela, I.; Pal, M.; Kerr, I. High strength tin-based overlay for medium and high-speed diesel engine bearing tribological applications. *Tribol. Int.* **2016**, *93*, 687–695. [[CrossRef](#)]
6. Aleshin, N.P.; Kobernik, N.V.; Mikheev, R.S.; Vaganov, V.E.; Reshetnyak, V.; Aborkin, A.V. Plasma–powder application of antifrictional babbitt coatings modified by carbon nanotubes. *Russ. Eng.* **2016**, *36*, 46–52. [[CrossRef](#)]
7. Fathy, N.; Ramadan, M. Influence of volume ratio of liquid to solid and low pouring temperature on interface structure of cast Babbitt-steel bimetal composite. *AIP Conf. Proc.* **2018**, *1966*, 020028. [[CrossRef](#)]
8. Belov, N.A.; Akopyan, T.K.; Gershman, I.S.; Stolyarova, O.O.; Yakovleva, A.O. Effect of Si and Cu additions on the phase composition, microstructure and properties of Al-Sn alloys. *J. Alloys Compd.* **2017**, *695*, 2730–2739. [[CrossRef](#)]
9. Diouf, P.; Jones, A. Investigation of Bond Strength in Centrifugal Lining of Babbitt on Cast Iron. *Metall. Mater. Trans. A* **2010**, *41*, 603–609. [[CrossRef](#)]
10. Ramadan, M.; Ayadi, B.; Rajhi, W.; Alghamdi, A.S. Influence of Tinning Material on Interfacial Microstructures and Mechanical Properties of Al12Sn4Si1Cu /Carbon Steel Bimetallic Castings for Bearing Applications. *Key Eng. Mater.* **2020**, *835*, 108–114. [[CrossRef](#)]
11. Zeren, A.; Feyzullahoglu, E.; Zeren, M. A study on tribological behaviour of tin-based bearing material in dry sliding. *Mater. Des.* **2007**, *28*, 318–323. [[CrossRef](#)]
12. Potekhin, B.A.; Il'yushin, V.V.; Khristolyubov, A.S. Effect of casting methods on the structure and properties of tin babbitt. *Met. Sci. Heat Treat* **2009**, *51*, 378–382. [[CrossRef](#)]
13. Gajmal, S.S.; Raut, D.N. An Investigation on Wear Behaviour of ASTM B23 tin-Based Babbitt Alloy Developed Through Microwave-Assisted Casting. *Int. Metalcast.* **2022**, *16*, 1995–2013. [[CrossRef](#)]
14. Dong, Q.; Yin, Z.; Li, H.; Zhang, X.; Jiang, D.; Zhong, N. Effects of Ag micro-addition on structure and mechanical properties of Sn-11Sb-6Cu Babbitt. *Mater. Sci. Eng. A* **2018**, *722*, 225–230. [[CrossRef](#)]
15. Tasgin, Y. Effect of MgO, Al<sub>2</sub>O<sub>3</sub> and FeCr<sub>2</sub>O<sub>4</sub> on microstructure and wear resistance of Babbitt metal (Sn–Sb–Cu). *Mater. Res. Express* **2019**, *6*, 046548. [[CrossRef](#)]
16. Ramadan, M.; Alghamdi, A.S.; Subhani, T.; Abdel Halim, K.S. Fabrication and Characterization of Sn-Based Babbitt Alloy Nanocomposite Reinforced with Al<sub>2</sub>O<sub>3</sub> Nanoparticles/Carbon Steel Bimetallic Material. *Materials* **2020**, *13*, 2759. [[CrossRef](#)] [[PubMed](#)]
17. Buchanan, V.E.; Molian, P.A.; Sudarshan, T.S.; Akers, A. Frictional behaviour of non-equilibrium Cu-Pb alloys. *Wear* **1991**, *146*, 241–256. [[CrossRef](#)]
18. Glaeser, W.A. Wear properties of heavy loaded Cu based bearing alloys. *J. Met.* **1983**, *35*, 50–55.
19. Ramadan, M.; Hafez, K.M. Interfacial microstructure and hardness of Sn-Based Babbitt/C93700 Cu-Pb-Sn bimetallic materials. *Mater. Today Proc.* **2021**, *45*, 5074–5080. [[CrossRef](#)]
20. Babu, M.; Krishna, A.R.; Suman, K. Review of Journal Bearing Materials and Current Trends. *Am. J. Mater. Sci. Technol.* **2015**, *4*, 72–83. [[CrossRef](#)]
21. Sturk, R.K.; Whitney, W.J. Fluid Film Bearing Materials. In *Encyclopedia of Tribology*; Wang, Q.J., Chung, Y.W., Eds.; Springer: Boston, MA, USA, 2013; pp. 1200–1216. [[CrossRef](#)]
22. Ramadan, M.; Hafez, K.M.; Alghamdi, A.S.; Ayadi, B.; Halim, K.S.A. Novel Approach for Using Ductile Iron as Substrate in Bimetallic Materials for Higher Interfacial Bonding Bearings. *Int. J. Met.* **2021**, *16*, 987–1000. [[CrossRef](#)]
23. Valeeva, A.K.; Valeev, I.S.; Fazlyakhmetov, R.F. Effect of structure of B83 babbitt on its wear. *J. Frict. Wear* **2014**, *35*, 311–315. [[CrossRef](#)]
24. Ji, X.; Chen, Y. Tribological Behavior of Babbitt Alloy Rubbing Against Si3N4 and Steel Under Dry Friction Condition. *J. Mater. Eng. Perform.* **2016**, *25*, 750–755. [[CrossRef](#)]
25. Fathy, N. Interfacial Microstructure and Bonding Area of Sn based Alloy-GG25 Gray Iron Bimetallic Material Using Flux, Sn, and Sn-Zn Interlayer Compound Casting, Engineering. *Technol. Appl. Sci. Res.* **2022**, *12*, 8416–8420. [[CrossRef](#)]
26. Mičić, M.; Đorđević, M.; Đajić, G. Characteristics of white metal slide layer bearings produced by cast cladding and weld cladding. *Metalurgija* **2006**, *12*, 225–236.
27. Ayadi, B.; Ramadan, M. Novel and simple technique for interfacial shear strength of liquid-solid compound casting specimen. *Mater. Today Proc.* **2021**, *47*, 2299–2304. [[CrossRef](#)]
28. Ramadan, M.; Fathy, N.; Abdel Halim, K.S.; Alghamdi, A.S. New trends and advances in bimetal casting technologies. *Int. J. Adv. Appl. Sci.* **2019**, *6*, 75–80. [[CrossRef](#)]
29. Altuner, S.; Kelesoglu, E. Production of Y<sub>2</sub>O<sub>3</sub> coated Al<sub>2</sub>O<sub>3</sub> reinforced aluminium matrix composites and the coating of interface effects over wettability properties. *J. Eng. Nat. Sci.* **2012**, *30*, 252–258.
30. Barykin, N.P.; Sadykov, F.A.; Aslanyan, I.R. Wear and failure of Babbitt bushes in steam turbine sliding bearings. *J. Mater. Eng. Perform.* **2000**, *9*, 110–115. [[CrossRef](#)]
31. Fathy, F. Interfacial Microstructure and Shear Strength Improvements of Babbitt–Steel Bimetal Composites Using Sn–Bi Interlayer via Liquid–Solid Casting. *Sustainability* **2023**, *15*, 804. [[CrossRef](#)]
32. Townsend, T.; Sabio, E.; Browning, N.; Osterloh, F. The oxygen evolution reaction: Water oxidation photocatalysis—Photocatalytic water oxidation with suspended alpha-Fe<sub>2</sub>O<sub>3</sub> particles—Effects of nanoscaling. In *Inorganic Metal Oxide Nanocrystal Photocatalysts for Solar Fuel Generation from Water*; Springer International Publishing: Berlin/Heidelberg, Germany, 2014; pp. 27–37.

33. Shivakumara, S.; Penki, T.; Munichandraiah, N. Preparation and electrochemical performance of porous hematite ( $\alpha$ - $\text{Fe}_2\text{O}_3$ ) nanostructures as supercapacitor electrode material. *J. Solid State Electrochem.* **2014**, *18*, 1057–1066. [[CrossRef](#)]
34. Gu, Y.; Zhao, X.C.; Li, Y.; Liu, Y.; Wang, Y.; Li, Z. Effect of nano- $\text{Fe}_2\text{O}_3$  additions on wettability and interfacial intermetallic growth of low-Ag content Sn-Ag-Cu solders on Cu substrates. *J. Alloys Compd.* **2015**, *627*, 39–47. [[CrossRef](#)]
35. Moille, G.; Chang, L.; Xie, W.; Rao, A.; Lu, X.; Davanço, M.; Bowers, J.E.; Srinivasan, K. Dissipative ksdks-V m, (laser photonics rev. 14(8)/2020). *Laser Photonics Rev.* **2020**, *14*, 2070043. [[CrossRef](#)]
36. Kong, L.; Zhang, L.; Bao, Y.; Liu, D.; Liu, S. Effect of Surface Roughness and Particle Size on Lubrication Mechanisms of  $\text{SiO}_2$  Nanoparticles. *Adv. Mater. Sci. Eng.* **2022**, *2022*, 7051650. [[CrossRef](#)]
37. Wang, Y.; Zhao, X.; Xie, X.; Gu, Y.; Liu, Y. Effects of nano- $\text{SiO}_2$  particles addition on the microstructure, wettability, joint shear force and the interfacial IMC growth of  $\text{Sn}_{3.0}\text{Ag}_{0.5}\text{Cu}$  solder. *J. Mater. Sci. Mater. Electron.* **2015**, *26*, 9387–9395. [[CrossRef](#)]
38. Iqbal, A.A.; Ismail, N.B. Mechanical Properties and Corrosion Behavior of Silica Nanoparticle Reinforced Magnesium Nanocomposite for Bio-Implant Application. *Materials* **2022**, *15*, 8164. [[CrossRef](#)]
39. Wu, H.; Bi, Q.; Zhu, S.; Yang, J.; Liu, W. Friction and wear properties of Babbitt alloy 16-16-2 under sea water environment. *Tribol. Int.* **2011**, *44*, 161–1167. [[CrossRef](#)]
40. Wu, H.R.; Bi, Q.L.; Yang, J.; Liu, W.M. Tribological performance of tin-based white metal ZChSnSb 8-8 under simulated sea water environment. *Mocaxue Xuebao/Tribology* **2011**, *31*, 271–277.
41. Zhao, X.; Wen, Y.; Li, Y.; Liu, Y.; Wang, Y. Effect of g- $\text{Fe}_2\text{O}_3$  nanoparticles size on the properties of Sn-1.0Ag0.5Cu nano-composite solders and joints. *J. Alloys Compd.* **2016**, *662*, 272–282. [[CrossRef](#)]
42. Babu, M.V.S.; Krishna, A.R.; Suman, K.N.S. Improvement of Tensile Behaviour of Tin Babbitt by Reinforcing with Nano Ilmenite and its Optimisation by using Response Surface Methodology. *Int. J. Manuf. Mater. Mech. Eng.* **2017**, *7*, 37–51.
43. Zhao, X.; Hai, X. Microstructure and tribological behaviour of the nickel-coated-graphite-reinforced Babbitt metal composite fabricated via selective laser melting. *Int. J. Min. Metall. Mater.* **2022**, *29*, 320. [[CrossRef](#)]
44. Kolev, M.; Drenchev, L.; Petkov, V. Wear analysis of an advanced Al- $\text{Al}_2\text{O}_3$  composite infiltrated with a tin-based alloy. *Metals* **2021**, *11*, 1692. [[CrossRef](#)]
45. Madej, M.; Madej, B.L.; Wisnios, J.H.; Weglowska, A. Effect of FSP on Tribological Properties of Grade B89 Tin Babbitt. *Materials* **2021**, *14*, 2627. [[CrossRef](#)]
46. Saboori, A.; Dadkhah, M.; Fino, P.; Pavese, M. An Overview of Metal Matrix Nanocomposites Reinforced with Graphene Nanoplatelets; Mechanical, Electrical and Thermophysical Properties. *Metals* **2018**, *8*, 423. [[CrossRef](#)]
47. Malaki, M.; Xu, W.; Kasar, A.K.; Menezes, P.L.; Dieringa Varma, H.; Gupta, M. Advanced Metal Matrix Nanocomposites. *Metals* **2019**, *9*, 330. [[CrossRef](#)]

**Disclaimer/Publisher’s Note:** The statements, opinions and data contained in all publications are solely those of the individual author(s) and contributor(s) and not of MDPI and/or the editor(s). MDPI and/or the editor(s) disclaim responsibility for any injury to people or property resulting from any ideas, methods, instructions or products referred to in the content.